

## ED-FEM multi-scale computation procedure for localized failure

Ivan Rukavina<sup>\*1</sup>, Adnan Ibrahimbegovic<sup>1a</sup>, Xuan Nam Do<sup>1</sup> and Damijan Markovic<sup>2</sup>

<sup>1</sup>*Université de Technologie de Compiègne / Sorbonne Universités, Laboratoire Roberval,  
Centre de Recherche Royallieu, 60 203 Compiègne, France*

<sup>2</sup>*EDF, DIPNN / Direction Technique, 19, rue Pierre Bourdeix, Lyon, France*

*(Received February 23, 2019, Revised March 19, 2019, Accepted March 21, 2019)*

**Abstract.** In this paper, we present a 2D multi-scale coupling computation procedure for localized failure. When modeling the behavior of a structure by a multi-scale method, the macro-scale is used to describe the homogenized response of the structure, and the micro-scale to describe the details of the behavior on the smaller scale of the material where some inelastic mechanisms, like damage or plasticity, can be defined. The micro-scale mesh is defined for each multi-scale element in a way to fit entirely inside it. The two scales are coupled by imposing the constraint on the displacement field over their interface. An embedded discontinuity is implemented in the macro-scale element to capture the softening behavior happening on the micro-scale. The computation is performed using the operator split solution procedure on both scales.

**Keywords:** multi-scale modeling; strong coupling; embedded discontinuity; operator split

### 1. Introduction

The first approach for multi-scale coupling is a numerical version of standard homogenization, where the standard form of the stiffness matrix is used, but with the elasticity tensor obtained by numerical homogenization. The latter is the product of computations at the micro-scale using the fine mesh on RVE - representative volume element (e.g., Feyel and Chaboche 2000, Geers *et al.* 2010). The alternative approach for multi-scale coupling is presented in Ibrahimbegovic and Markovic (2003) and Ibrahimbegovic (2009), where the micro-scale mesh is placed inside a macro-element. Contrary to homogenization, we obtain the element residual and tangent stiffness matrix directly. The previously proposed numerical homogenization model is adequate for representing elastic behavior and hardening, but not for the localized failure. When a localized failure occurs on the micro-scale it cannot be properly transferred to the macro-scale, and the macro-scale element is not able to adequately represent the displacement jump.

To overcome this problem, an embedded discontinuity multi-scale procedure is proposed. In this way, the localized failure can be represented on the macro-scale. The proposed procedure, described in detail, represents the main contribution and novelty in this paper.

---

<sup>\*</sup>Corresponding author, Ph.D. Student, E-mail: [ivan.rukavina@utc.fr](mailto:ivan.rukavina@utc.fr)

<sup>a</sup>Chair for Computational Mechanics, Professor, E-mail: [adnan.ibrahimbegovic@utc.fr](mailto:adnan.ibrahimbegovic@utc.fr)

## 2. Multi-scale formulation

In the proposed multi-scale coupling, the two scales are strongly coupled, which means that they are exchanging information during the whole analysis, and the computation advances simultaneously on both scales. At each time step, both macro and micro-scale computations are executed, and only when convergence is obtained at both scales, we advance to the next time step. The finite element method is used at both scales, which adds to the generality of the method and simplicity of its implementation. A micro-scale mesh, finitely smaller than the macro-scale mesh, is placed inside each of the macro-scale elements. Hence, the constitutive equation is not defined on the macro element, and its element arrays are obtained from the micro-scale computations. The two scales are strongly coupled using displacement based coupling, where the micro-scale displacements on the interface are imposed by the macro-scale displacements.

For scale coupling, the localized Lagrange multiplier method (Park *et al.* 2002) is used. It allows to replace the standard computation of the element tangent stiffness matrices and the residual vectors by an assembly of micro-scale contributions which are statically condensed at the macro-scale (Hautefeuille *et al.* 2012). The finite element models on the micro-scale communicate between each other only through the degrees of freedom defined at the macro-scale. In this way, micro-scale computations are independent of each other and can be executed in parallel, significantly reducing execution time.

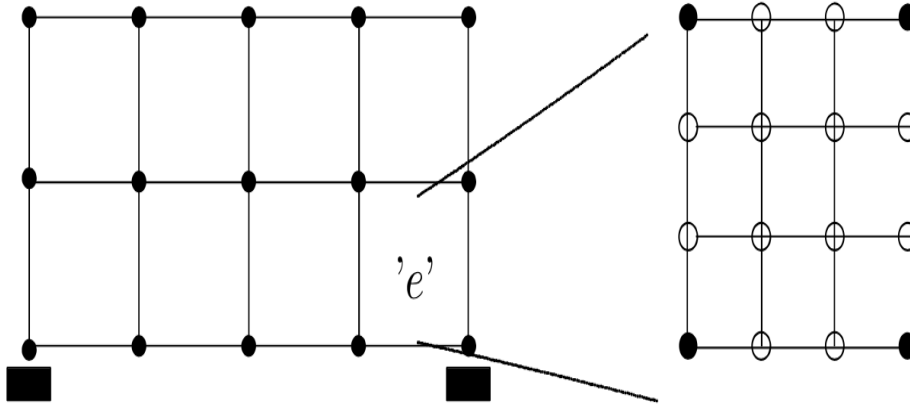


Fig. 1 Multiscale model with FE mesh at both the macro and micro-scale (according to Ibrahimbegovic and Markovic 2003)

For the variational formulation of a multi-scale problem, the total energy can be written as a sum of energies

$$\Pi(u^M, u^m, \lambda, \bar{\xi}_k) = \Pi^M + \Pi^m + \Pi^{\Gamma^{Mm}} \quad (1)$$

where  $\Pi^M$  is the strain energy at the macro-scale,  $\Pi^m$  strain energy at the micro-scale and  $\Pi^{\Gamma^{Mm}}$  is the energy at the interface between the two scales.

The external forces are assumed to apply only at the macro-scale, while the constitutive laws and the internal variables are defined only at the micro-scale. Hence, each of the energies can be written as

$$\begin{aligned}
\Pi^M &= - \int_{\Omega^M} u^M \cdot b^M dV - \int_{\Gamma_\sigma^M} u^M \cdot \bar{t} dA \\
\Pi^m &= \int_{\Omega^m} \psi^m(u^m, \xi_k) dV \\
\Pi^{\Gamma^{Mm}} &= \int_{\Gamma^{Mm}} \lambda \cdot (u^M - u^m) dA
\end{aligned} \tag{2}$$

where  $u^M$  and  $u^m$  are macro and micro-scale displacements respectively,  $b^M$  represents volumetric forces,  $\bar{t}$  is the traction force,  $\lambda$  is the Lagrange multiplier that allows for scale coupling, and  $\psi^m$  is the strain energy density.

Since nonlinear inelastic behavior is considered, an incremental-iterative analysis (e.g., Ibrahimbegovic 2009) is used to obtain the final solution. In any typical increment, the central problem of multi-scale analysis can be posed as

For given  $u_n^M = u^M(x^M, t_n)$ ,  $u_n^m = u^m(x^m, t_n)$ ,  $\lambda_n = \lambda(x^M, t_n)$ ,  $\xi_{k,n} = \xi_k(x^m, t_n)$ ,  $h = t_{n+1} - t_n$  find  $u_{n+1}^M$ ,  $u_{n+1}^m$ ,  $\lambda_{n+1}$ ,  $\xi_{k,n+1}$ , such that

$$\begin{aligned}
0 &= \left. \frac{d}{d\epsilon} \right|_{\epsilon=0} \Pi^m(u_{n+1}^m + \epsilon w^m, \cdot) \equiv G^m(u_{n+1}^m, \lambda_{n+1}, \xi_{k,n+1}; w^m) = \\
&= \int_{\Omega^m} \nabla^s w^m \cdot \hat{\sigma}^m(u_{n+1}^m, \xi_{k,n+1}) dV - \int_{\Gamma^{Mm}} w^m \cdot \lambda dA
\end{aligned} \tag{3}$$

$$\begin{aligned}
0 &= \left. \frac{d}{d\epsilon} \right|_{\epsilon=0} \Pi^M(u_{n+1}^M + \epsilon w^M, \cdot) \equiv G^M(u_{n+1}^M, \lambda_{n+1}; w^M) = \\
&= \int_{\Gamma^{Mm}} w^M \cdot \lambda dA - \int_{\Omega^M} w^M \cdot b dV - \int_{\Gamma_\sigma^M} w^M \cdot \bar{t} dA
\end{aligned} \tag{4}$$

$$\begin{aligned}
0 &= \left. \frac{d}{d\epsilon} \right|_{\epsilon=0} \Pi^{Mm}(\lambda_{n+1} + \epsilon \nu, \cdot) \equiv G^{Mm}(u_{n+1}^M, u_{n+1}^m, \nu) = \\
&= \int_{\Gamma^{Mm}} \nu \cdot (u_{n+1}^M - u_{n+1}^m) dA
\end{aligned} \tag{5}$$

with  $\xi_{k,n+1} = \xi_{k,n} + h\hat{f}(u_{n+1}^M, u_{n+1}^m, \lambda_{n+1}, \xi_{k,n+1})$

The standard finite element shape functions for the isoparametric Q4 element (e.g., Ibrahimbegovic 2009) are used at the macro-scale

$$N_a(\xi, \eta) = \frac{1}{4}(1 + \xi_a \xi)(1 + \eta_a \eta), \quad a = 1, 2, 3, 4 \tag{6}$$

where  $\xi_a$  and  $\eta_a$  are the coordinates of node  $a$ .

At the micro-scale, the constant strain triangle (CST) element with one integration point is used. We implemented the damage model with incompatible mode, as described in Do and Ibrahimbegovic (2018) and Ibrahimbegovic and Brancherie (2003).

The displacement field approximations at the micro and macro-scale, and localized Lagrange multipliers are calculated with standard finite element approximations, which can be written as

$$\begin{aligned}
\mathbf{u}_{n+1}^m \Big|_{\Omega^{m,e}}(\mathbf{x}^m) &= \sum_{a=1}^{n_{el}^m} \mathbf{N}_a^{m,e}(\mathbf{x}^m) \mathbf{d}_{a,n+1}^m \\
\mathbf{u}_{n+1}^M \Big|_{\Gamma^{Mm,E}}(\mathbf{x}^m) &= \sum_{a \in \Gamma^{Mm,E}} \mathbf{N}_a^{M,E}(x^m) \mathbf{d}_{a,n+1}^{M,E} \\
\lambda_{n+1} \Big|_{\Gamma^{Mm,E}}(\mathbf{x}^m) &= \sum_{a \in \Gamma^{Mm,E}} \mathbf{P}_a^{M,E}(\mathbf{x}^m) \beta_{a,n+1}
\end{aligned} \tag{7}$$

Keeping in mind the above stated approximations, the central problem can now be rewritten as follows

For given  $d_n^{M,E}, d_n^m, \beta_n, \xi_{k,n}; \forall \Omega^{M,E}$   
find  $d_{n+1}^{M,E}, d_{n+1}^m, \beta_{n+1}, \xi_{k,n+1}$ ,  
such that ( $\forall e \in [1, n_{el}^m], \forall E \in [1, n_{el}^M]$ )

$$\begin{aligned}
0 &= r^m(d_{n+1}^m, \beta_{n+1}, \xi_{k,n+1}) = \\
&= \mathbb{A}_{e=1}^{n_{elem}^m} \left[ \int_{\Omega^{m,e}} B^{mT} \cdot \hat{\sigma}(d_{n+1}^m, \xi_{k,n+1}) dV \right] - \int_{\Gamma^{Mm,E}} N^{m,eT} P^{M,E} \beta_{n+1} dA
\end{aligned} \tag{8}$$

$$\begin{aligned}
0 &= r^M(d_{n+1}^M, \beta_{n+1}) = \\
&= \mathbb{A}_{E=1}^{n_{elem}^M} \left[ \int_{\Gamma^{M,E}} N^{M,ET} P^{M,E} \beta_{n+1} dA - \int_{\Omega^{M,E}} N^{M,ET} b dV - \int_{\Gamma^{M,E}} N^{M,ET} \bar{t} dA \right]
\end{aligned} \tag{9}$$

$$0 = p^{M,E}(d_{n+1}^{M,E}, d_{n+1}^m, \beta_{n+1}) = \int_{\Omega^{M,E}} P^{ET} (N^{M,E} d^{M,E} - N^m d^m) dA \tag{10}$$

with  $\xi_{k,n+1} = \xi_{k,n} + h\hat{f}(d_{n+1}^{M,E}, d_{n+1}^m, \lambda_{n+1}, \xi_{k,n+1})$

The localized Lagrange multipliers enforce that the displacements of the interface nodes at the micro-scale are calculated as a linear interpolation of the nodal values of displacements at the macro-scale. This can be achieved by choosing the Dirac delta functions  $\delta(x - x_a)$  centered upon the micro-scale interface nodes  $x_a \in \Gamma^{M,E}$ . By introducing it into (10), we can obtain

$$p_a^M = \bar{\mathbf{d}}_{a,n+1}^m - \sum_b N_b^{M,E}(x_a) \mathbf{d}_{b,n+1}^{M,E} = 0 \tag{11}$$

Finally, the micro-scale nodal displacement vector on the interface can be written as

$$\bar{\mathbf{d}}_{n+1}^m \Big|_{\Gamma^{M,E}} = \mathbf{T}^E \mathbf{d}_{n+1}^{M,E} \tag{12}$$

where  $T^E$  is the connectivity matrix, and  $d_{n+1}^{M,E}$  are macro-scale nodal displacements.

The connectivity matrix  $T^E$  is based on the particular values of macro-scale shape functions which correspond to the interface nodes. Namely, that matrix is constructed by simply introducing the isoparametric coordinates of each micro-scale node on the interface into the macro-scale shape

functions  $N_a$ .

The standard finite element system of equations for computing the increment of the displacement field on the micro-scale can be written as

$$\begin{bmatrix} \bar{\mathbf{K}} & \bar{\mathbf{K}}^T \\ \bar{\mathbf{K}} & \mathbf{K} \end{bmatrix} \begin{bmatrix} \Delta \bar{\mathbf{d}} \\ \Delta \mathbf{d} \end{bmatrix} = - \begin{bmatrix} \bar{\mathbf{r}} \\ \mathbf{r} \end{bmatrix} \quad (13)$$

where  $\bar{\mathbf{K}}$  is the part of the stiffness matrix related only to interface nodes,  $\bar{\mathbf{K}}$  is related to interface nodes in relation to free nodes and  $\mathbf{K}$  is related only to free nodes. In the same way,  $\Delta \bar{\mathbf{d}}$  and  $\bar{\mathbf{r}}$  are the displacement increments and residuals of the interface nodes, and  $\Delta \mathbf{d}$  and  $\mathbf{r}$  are displacement increments and residuals of free nodes.

The static condensation (e.g., Ibrahimbegovic 2009) can be performed on the previous system of equations. First, the displacement field increment of free nodes can be expressed as

$$\Delta \mathbf{d} = \mathbf{K}^{-1}(-\mathbf{r} - \bar{\mathbf{K}}\Delta \bar{\mathbf{d}}) \quad (14)$$

Introducing (14) to the first equation from (13) we can obtain

$$\left( \bar{\mathbf{K}} - \bar{\mathbf{K}}^T \mathbf{K}^{-1} \bar{\mathbf{K}} \right) \Delta \bar{\mathbf{d}} = -\bar{\mathbf{r}} + \bar{\mathbf{K}}^T \mathbf{K}^{-1} \mathbf{r} \quad (15)$$

Then, the statically condensed stiffness matrix and residual obtained at the micro-scale can be written as

$$\begin{aligned} \tilde{\mathbf{K}}^m &= \left( \bar{\mathbf{K}} - \bar{\mathbf{K}}^T \mathbf{K}^{-1} \bar{\mathbf{K}} \right) \\ \tilde{\mathbf{r}}^m &= -\bar{\mathbf{r}} + \bar{\mathbf{K}}^T \mathbf{K}^{-1} \mathbf{r} \end{aligned} \quad (16)$$

After the computations on the micro-scale have converged, the final values of the condensed stiffness matrix and residual are used to compute the values of the stiffness matrix and residual to be used at the macro-scale

$$\begin{aligned} \mathbf{K}_{n+1}^{M,E} &= \mathbf{T}^{E,T} \tilde{\mathbf{K}}_{n+1}^m \mathbf{T}^E \\ \mathbf{r}_{n+1}^{M,E} &= \mathbf{T}^{E,T} \tilde{\mathbf{r}}_{n+1}^m \end{aligned} \quad (17)$$

When the values of the macro-scale stiffness matrix and residual are computed, they are used to update the values of the macro-scale displacement field. The standard finite element system of equations needs to be solved

$$\mathbf{K}_{n+1}^M \Delta \mathbf{d}_{n+1}^M = -\mathbf{r}_{n+1}^M \quad (18)$$

### 3. Multi-scale formulation for localized failure

The multi-scale formulation described in the previous chapter cannot take into account the crack propagation. So the localized failure that can happen on the micro-scale cannot be transferred to the macro-scale. In order to allow for the multi-scale model to represent localized failure, the corresponding incompatible mode is introduced inside the macro-scale element. In this way, the displacement discontinuity can be properly transferred from micro to macro-scale. The discontinuity is positioned at the center of the Q4 element. Vectors  $n$  and  $m$  are normal and

tangential vectors at the discontinuity. In this paper, for simplicity, we will illustrate such model for a simple tension test, which can take into account only the crack opening in mode I. Thus, only the normal direction vector will have a non-zero value. The element domain is divided into two sub-domains:  $\Omega^{e-}$  and  $\Omega^{e+}$ , as shown in Fig. 2(a). Hence, the incompatible mode function can be written as

$$M(\xi, \eta) = H_{\Gamma}(\xi, \eta) - \sum_{b \in \Omega^{e+}} N_b(\xi, \eta) \quad (19)$$

where  $H_{\Gamma}$  is the Heaviside step function defined as

$$H_{\Gamma} = \begin{cases} 0, & (\xi, \eta) \in \Omega^{e-} \\ 1, & (\xi, \eta) \in \Omega^{e+} \end{cases} \quad (20)$$

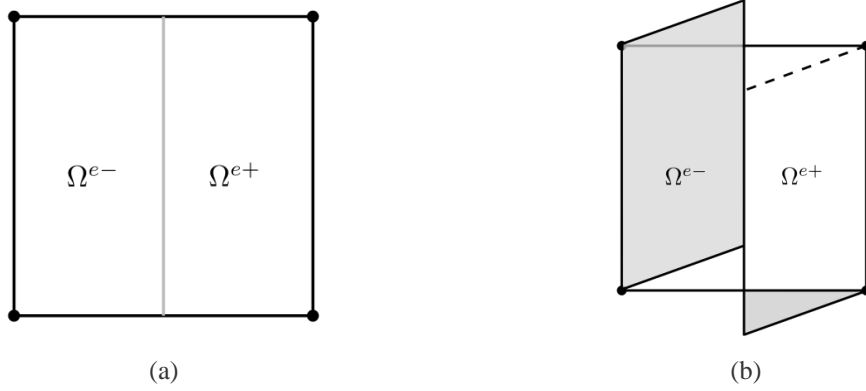


Fig. 2(a) Q4 isoparametric element with two sub-domains related to the displacement jump; (b) Incompatible mode shape function  $\mathbf{M}$  for the discontinuity in the middle of the element

Now, the macro-scale displacement field from (7) can be rewritten as

$$\mathbf{u}_{n+1}^M \Big|_{\Gamma^{Mm,E}}(\mathbf{x}^m) = \sum_{a \in \Gamma^{Mm,E}} \mathbf{N}_a^{M,E}(\mathbf{x}^m) \mathbf{d}_{a,n+1}^{M,E} + \mathbf{M}^{M,E} \alpha_{n+1}^{M,E} \quad (21)$$

where  $\alpha_{n+1}^{M,E}$  is the value of the displacement discontinuity.

Now the macro-scale displacement field approximation can be introduced into (10)

$$\begin{aligned} 0 &= \mathbf{p}^{M,E}(\mathbf{d}_{n+1}^{M,E}, \mathbf{d}_{n+1}^m, \beta_{n+1}) = \\ &= \int_{\Omega^{M,E}} \mathbf{P}^{E^T} (\mathbf{N}^{M,E} \mathbf{d}^{M,E} + \mathbf{M}^{M,E} \alpha^{M,E} - \mathbf{N}^{m,e} \mathbf{d}^m) dA \end{aligned} \quad (22)$$

The displacement field on the micro-scale interface nodes is now a function of both the macro-scale displacement field and the displacement discontinuity

$$\mathbf{p}_a^M = \bar{\mathbf{d}}_{a,n+1}^m - \sum_b \mathbf{N}_b^{M,E}(x_a) \mathbf{d}_{b,n+1}^{M,E} - \mathbf{M}^{M,E}(x_a) \alpha_{n+1}^{M,E} = 0 \quad (23)$$

The final expression used to compute the micro-scale nodal displacement field on the interface can be written as

$$\bar{\mathbf{d}}_{n+1}^m \Big|_{\Gamma^{M,E}} = \mathbf{T}^E \mathbf{d}_{n+1}^{M,E} + \mathbf{S}^E \alpha_{n+1}^{M,E} \quad (24)$$

where  $\mathbf{S}^E$  is the connectivity matrix for the incompatible mode, and  $\alpha_{n+1}^{M,E}$  is the displacement jump.

The additional connectivity matrix  $\mathbf{S}^E$  is constructed based on the macro-scale incompatible mode function. The isoparametric coordinates of each micro-scale interface node are introduced into the macro-scale incompatible mode function  $M$ .

The system of equations that needs to be solved on the macro-scale can be defined as

$$\begin{bmatrix} \mathbf{K}^M & \mathbf{F}^M \\ \mathbf{F}^{M,T} & \mathbf{H}^M \end{bmatrix} \begin{bmatrix} \Delta \mathbf{d}^M \\ \Delta \alpha^M \end{bmatrix} = - \begin{bmatrix} \mathbf{r}^M \\ \mathbf{h}^M \end{bmatrix} \quad (25)$$

To construct the macro-scale stiffness matrix needed for solving the macro-scale system of equations, submatrices  $\mathbf{K}^M$ ,  $\mathbf{F}^M$  and  $\mathbf{H}^M$  are computed as

$$\begin{aligned} \mathbf{K}_{n+1}^{M,E} &= \mathbf{T}^{E,T} \tilde{\mathbf{K}}_{n+1}^m \mathbf{T}^E \\ \mathbf{F}_{n+1}^{M,E} &= \mathbf{T}^{E,T} \tilde{\mathbf{K}}_{n+1}^m \mathbf{S}^E \\ \mathbf{H}_{n+1}^{M,E} &= \mathbf{S}^{E,T} \tilde{\mathbf{K}}_{n+1}^m \mathbf{S}^E \end{aligned} \quad (26)$$

This corresponds to the way this submatrices are computed in the standard finite element procedure on the global level for the incompatible mode method

$$\begin{aligned} \mathbf{K}_{n+1}^e &= \int_{\Omega^e} \mathbf{B}^{e,T} \mathbf{C}_{n+1}^{ed,(i)} \mathbf{B}^e d\Omega \\ \mathbf{F}_{n+1}^e &= \int_{\Omega^e} \mathbf{B}^{e,T} \mathbf{C}_{n+1}^{ed,(i)} \tilde{\mathbf{G}}^e d\Omega \\ \mathbf{H}_{n+1}^e &= \int_{\Omega^e} \tilde{\mathbf{G}}^{e,T} \mathbf{C}_{n+1}^{ed,(i)} \tilde{\mathbf{G}}^e d\Omega \end{aligned} \quad (27)$$

where  $\mathbf{B}^e$  is the matrix containing the shape functions derivatives,  $\tilde{\mathbf{G}}^e$  is the matrix containing incompatible mode function derivatives, and  $\mathbf{C}^{ed}$  is the tangent elasto-damage tensor.

In the same way, the macro-scale residuals are computed using the values of micro-scale residuals and transformation matrices  $\mathbf{T}$  and  $\mathbf{S}$

$$\begin{aligned} \mathbf{r}_{n+1}^{M,E} &= \mathbf{T}^{E,T} \tilde{\mathbf{r}}_{n+1}^m \\ \mathbf{h}_{n+1}^{M,E} &= \mathbf{S}^{E,T} \tilde{\mathbf{r}}_{n+1}^m \end{aligned} \quad (28)$$

In the standard finite element procedure, the values of residuals are computed as

$$\begin{aligned} \mathbf{r}_{n+1}^e &= \int_{\Omega^e} \mathbf{B}^{e,T} \sigma(d, \alpha) d\Omega \\ \mathbf{h}_{n+1}^e &= \int_{\Omega^e} \tilde{\mathbf{G}}^e \sigma(d, \alpha) d\Omega \end{aligned} \quad (29)$$

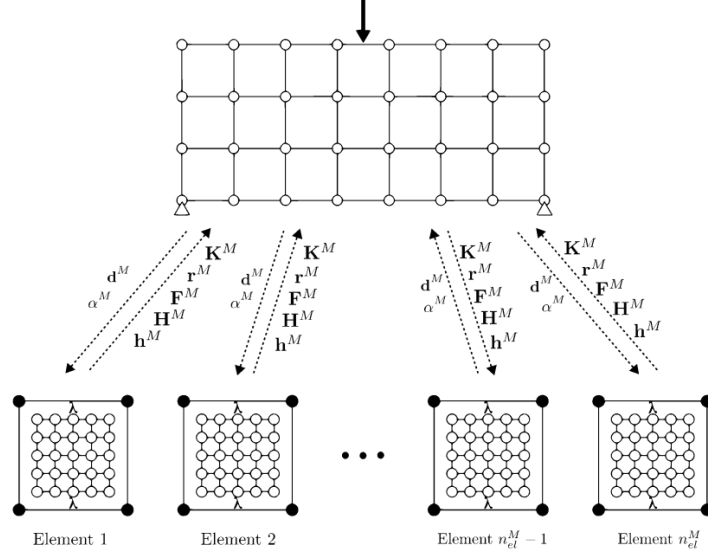


Fig. 3 The macro-scale and micro-scale data transferred between the scales in every time step (according to Ibrahimbegovic and Markovic (2003) with added data for the incompatible mode)

The system of Eq. (25) is solved using the operator split procedure (e.g., Ibrahimbegovic 2009). First, the values of the macro-scale displacements are fixed, while the correct value of  $\alpha^M$  has to be calculated iteratively. Each iteration consists of calling the micro-scale computations with the imposed micro-scale interface displacement field as a function of the macro-scale displacement field and displacement discontinuity field. After each micro-scale iteration, the value of the macro-scale displacement jump increment is computed from the equation

$$\mathbf{H}_{n+1}^{M,E(i,j)} \Delta \alpha_{n+1}^{M,E(i,j)} = \mathbf{h}_{n+1}^{M,E(i,j)} \quad (30)$$

and then the value of the macro-scale displacement jump is updated as

$$\alpha_{n+1}^{M,E(i,j+1)} = \alpha_{n+1}^{M,E(i,j)} + \Delta \alpha_{n+1}^{M,E(i,j)} \quad (31)$$

If the value of the residual  $\mathbf{h}_{n+1}^{M,E(i,j)}$  obtained by the micro-scale computations is smaller than the chosen tolerance, we can stop the iterations, since the correct value of  $\alpha_{n+1}^{M,E(i)}$  is reached. If the residual  $\mathbf{h}_{n+1}^{M,E(i,j)}$  is greater than the tolerance, we start another micro-scale iteration ( $j$ ) to update the value of  $\alpha_{n+1}^{M,E(i)}$ . The micro-scale computation is then executed with the updated value of  $\alpha_{n+1}^{M,E(i,j+1)}$  from the current iteration, so the micro-scale interface displacement field is updated again using (24). The detailed flow-chart of the proposed multi-scale operator split solution procedure is shown in Algorithm 1.

After the value of  $\alpha^M$  has converged, the second step of the operator split procedure is activated. In the second step the value of  $\alpha^M$  is fixed and the values of the macro-scale displacement field iterative contributions are computed as

$$[\mathbf{K}_{n+1}^{M(i)} - \mathbf{F}_{n+1}^{M(i)} (\mathbf{H}_{n+1}^{M(i)})^{-1} \mathbf{F}_{n+1}^{M(i)T}] \Delta \mathbf{d}_{n+1}^{M(i)} = -\mathbf{r}_{n+1}^{M(i)} \quad (32)$$

followed by the corresponding update of the macro displacements

$$\mathbf{d}_{n+1}^{M(i+1)} = \mathbf{d}_{n+1}^{M(i)} + \Delta \mathbf{d}_{n+1}^{M(i)} \quad (33)$$

```

for  $n=0,1,2,\dots$  do
  for  $(i)=1,2,\dots$  do
    for  $(j)=1,2,\dots$  do
      for  $E=1,2,\dots,n_{el}^M$  do
         $\bar{\mathbf{d}}_{n+1}^{m(i,j,1)}|_{\Gamma^{M,E}} = \mathbf{T}^E \mathbf{d}_{n+1}^{M,E(i)} + \mathbf{S}^E \boldsymbol{\alpha}_{n+1}^{M,E(i,j)}$ 
        for  $(k)=1,2,\dots$  do
           $\mathbb{A}_{e=1}^{n_{el}^m} [\mathbf{K}_{n+1}^{m,e(i,j,k)} (\mathbf{d}_{n+1}^{m,e(i,j,k+1)} - \mathbf{d}_{n+1}^{m,e(i,j,k)}) = -\mathbf{r}_{n+1}^{m,e(i,j,k)}]$ 
          if  $\|\mathbf{r}_{n+1}^{m,e(i,j,k+1)}\| > tol$  then
             $(k) = (k) + 1$ 
          else
             $\mathbf{r}_{n+1}^{M,E(i,j)} = \mathbf{T}^{E,T} \tilde{\mathbf{r}}_{n+1}^m$ 
             $\mathbf{h}_{n+1}^{M,E(i,j)} = \mathbf{S}^{E,T} \tilde{\mathbf{r}}_{n+1}^m$ 
             $\mathbf{K}_{n+1}^{M,E(i,j)} = \mathbf{T}^{E,T} \tilde{\mathbf{K}}_{n+1}^m \mathbf{T}^E$ 
             $\mathbf{F}_{n+1}^{M,E(i,j)} = \mathbf{T}^{E,T} \tilde{\mathbf{K}}_{n+1}^m \mathbf{S}^E$ 
             $\mathbf{H}_{n+1}^{M,E(i,j)} = \mathbf{S}^{E,T} \tilde{\mathbf{K}}_{n+1}^m \mathbf{S}^E$ 
            exit loop
          end
        end
         $E = E + 1$ 
      end
      if  $\|\mathbf{h}_{n+1}^{M,E(i,j)}\| > tol$  then
         $\Delta \boldsymbol{\alpha}_{n+1}^{M,E(i,j)} = \mathbf{H}_{n+1}^{M,E(i,j)^{-1}} \mathbf{h}_{n+1}^{M,E(i,j)}$ 
         $\boldsymbol{\alpha}_{n+1}^{M,E(i,j+1)} = \boldsymbol{\alpha}_{n+1}^{M,E(i,j)} + \Delta \boldsymbol{\alpha}_{n+1}^{M,E(i,j)}$ 
         $(j) = (j) + 1$ 
      else
        exit loop
      end
    end
     $\mathbb{A}_{E=1}^{n_{el}^M} [(\mathbf{K}_{n+1}^{M,E(i)} - \mathbf{F}_{n+1}^{M,E(i)} \mathbf{H}_{n+1}^{M,E(i)^{-1}} \mathbf{F}_{n+1}^{M,E(i)T}) (\mathbf{d}_{n+1}^{M,E(i+1)} - \mathbf{d}_{n+1}^{M,E(i)}) = -\mathbf{r}_{n+1}^{M,E(i)}]$ 
    if  $\|\mathbf{r}_{n+1}^{M,E(i)}\| > tol$  then
       $(i) = (i) + 1$ 
    else
      exit loop
    end
  end
   $n = n + 1$ 
end

```

Algorithm 1: Operator split multi-scale iterative solution procedure

#### 4. Software implementation

For implementing the proposed procedure, we use the Finite Element Analysis Program (FEAP) (see Zienkiewicz *et al.* 2013). It is chosen because different material behaviors can be easily implemented by changing the existing code. To simulate behavior on both macro and micro-scale, two different version of FEAP code are implemented (as explained in Niekamp *et al.* 2009). macroFEAP is used on the macro-scale, and its behavior is different from the standard version in the sense that it can initiate the execution of microFEAP instances and use the obtained results. microFEAP was modified in a way that it can take the input data, and its execution can be controlled from the macroFEAP code. For coupling the two codes and exchanging information between them, Component Template Library (CTL) is used (see Niekamp *et al.* 2014).

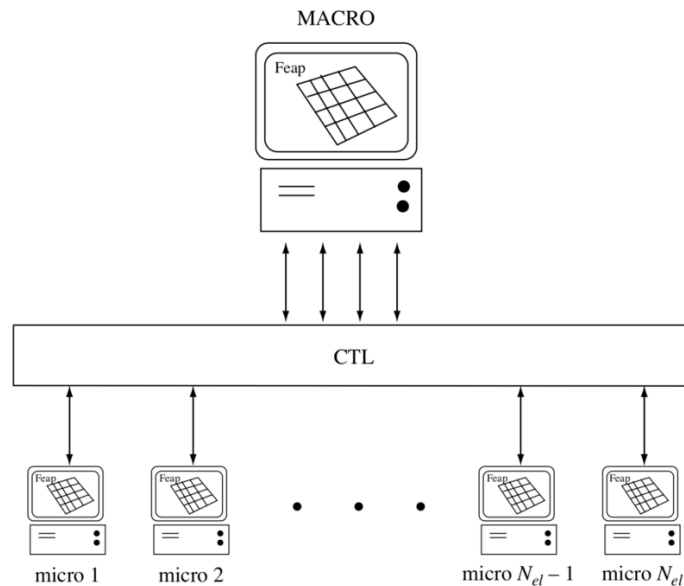


Fig. 4 Parallel execution and code coupling with CTL (according to Niekamp *et al.* 2009)

To solve a multi-scale problem example, one instance of macroFEAP process and  $n_{elem}^M$  instances of microFEAP processes are created (as shown in Fig. 4), where  $n_{elem}^M$  is the number of elements in the macro mesh. microFEAP instances are executed in parallel, as they do not need any communication between them, since they are not using the same data. Input data for the macro-scale consists of defining the macro mesh and boundary conditions. The constitutive properties of the material do not have to be defined, as they will be obtained from the micro-scale computations. On the micro-scale, the mesh has to be defined, but no boundary conditions, as those are automatically imposed by the multi-scale solution procedure.

In each time step, the macroFEAP instance transfers the nodal displacement field and displacement discontinuity field for each macro-scale element to the corresponding microFEAP instance using CTL. Based on that input, microFEAP instances solve the imposed problem in parallel. After obtaining the final values of the stiffness matrix and residual, they transfer them

back to macroFEAP. Only when all microFEAP instances finished their execution and results are transferred, macroFEAP can continue its execution.

## 5. Numerical examples

### 5.1 Validation examples for the proposed multi-scale approach

To validate the theoretical formulation with numerical examples, we have chosen a simple tension test. The results for the proposed multi-scale method are compared against the monolithic solution and previously developed multi-scale method. The goal was to prove that the embedded discontinuity multi-scale method can represent the localized failure and produce the same quality results as the monolithic solution. The simple tension test with boundary conditions and imposed displacement is shown in Fig. 5.

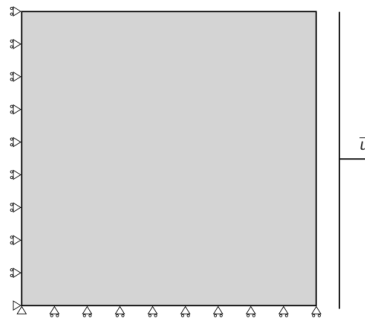


Fig. 5 Simple tension test - boundary conditions

The mesh for the mono-scale example (shown in Fig. 6(a)) consist of 18 x 18 CST elements. The weakened elements that are going to crack first are shown in gray. The macro-scale mesh (shown in Fig. 6(b)) of the multi-scale example has the same dimensions as the mono-scale mesh, and consists of 3 x 3 Q4 elements.

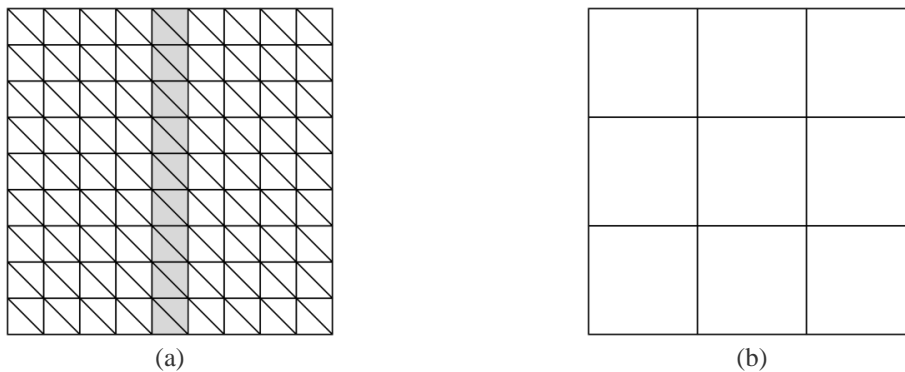


Fig. 6(a) Mono-scale mesh; (b) Macro-scale mesh

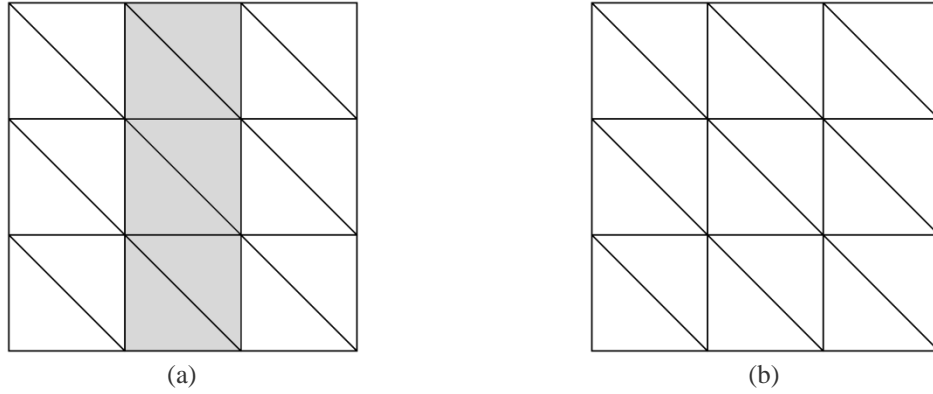


Fig. 7(a) Micro-scale mesh with weakened elements; (b) Micro-scale mesh without weakened elements

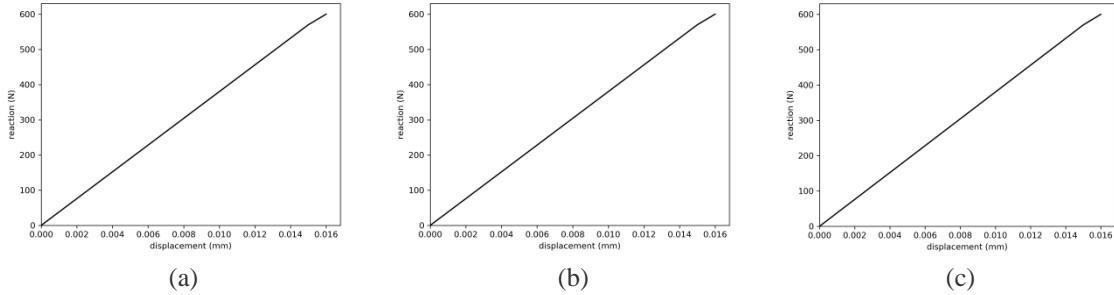


Fig. 8 Force-displacement diagrams for elastic response: (a) Mono-scale; (b) Multi-scale; (c) ED-FEM multi-scale

Inside each of the macro-scale elements there is a micro-scale mesh that consists of  $6 \times 6$  CST elements. A different micro-scale mesh can be defined for each macro-scale element. The three central macro-scale elements (where the crack should appear) contain the micro-mesh shown in Fig. 7(a). The other six macro-scale elements on the left and the right side contain the micro-mesh without the weakened elements (shown in Fig. 7(b)). For the multi-scale example, there are boundary conditions imposed only on the macro-scale.

In this way, the mono-scale and the multi-scale examples have the same total number of CST elements, the same position of the weakened elements and the same dimensions, and therefore should behave in the same way. The central column of the weakened CST elements inside the micro-scale mesh coincides with the displacement discontinuity of the Q4 macro-scale element. The element used for this analysis is the CST damage element described in Do and Ibrahimbegovic (2018).

We have chosen the following material parameters for the CST damage element: the Young's modulus  $E = 38\,000$  MPa, the hardening modulus  $\bar{K} = 1000$  MPa, the Poisson's ratio  $\nu = 0$ , the limit stress for hardening  $\bar{\sigma} = 2$  MPa, the ultimate stress  $\bar{\sigma} = 2.5$  MPa, the ratio of the softening parameter and the ultimate stress is 20, and the ratio between the tangential and the normal direction ultimate stress is 0.3. The dimensions of the mesh are  $300 \times 300$  mm and the imposed displacement  $\bar{u} = 1$  mm.

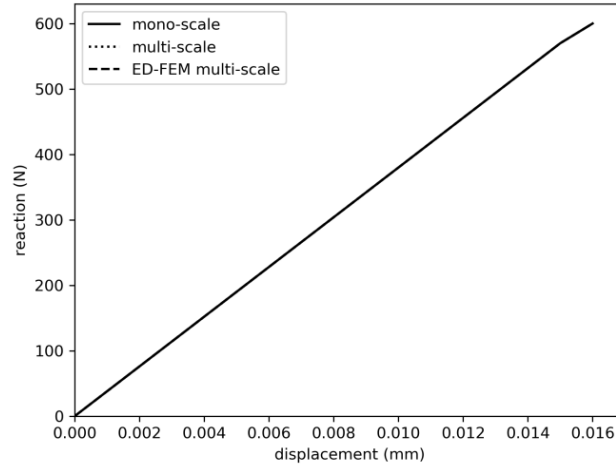


Fig. 9 Superposed force-displacement diagrams for elastic response computed by three different methods

### 5.2 Elastic response

When the stress is small enough and only elastic response is obtained, the results for mono-scale and both multi-scale methods produce the same force-displacement diagram as shown in Fig. 8. Both multi-scale methods are giving the same results since no crack appears on the micro-scale, so there is no need to represent it on the macro-scale. Only the stiffness matrix  $\mathbf{K}^M$  and the residual  $\mathbf{h}^M$  are transferred from the micro to the macro-scale.

### 5.3 Elasto-damage with hardening

When the structure enters the hardening phase, the force-displacement diagrams for all three methods are still the same, as shown in Fig. 10. The only change compared to the elastic phase are the values of the stiffness matrix  $\mathbf{K}^M$  due to the introduction of the hardening modulus  $\bar{K}$ . These changes are successfully captured and transferred from the micro to the macro-scale for both multi-scale methods.

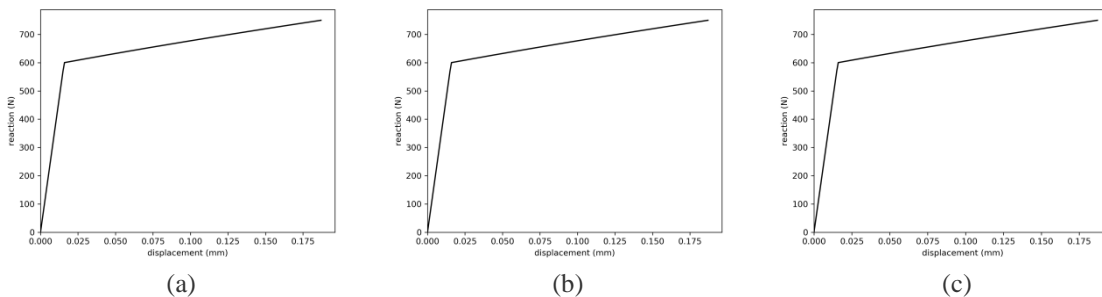


Fig. 10 Force-displacement diagrams for elasto-damage with hardening: (a) Mono-scale; (b) Multi-scale; (c) ED-FEM multi-scale

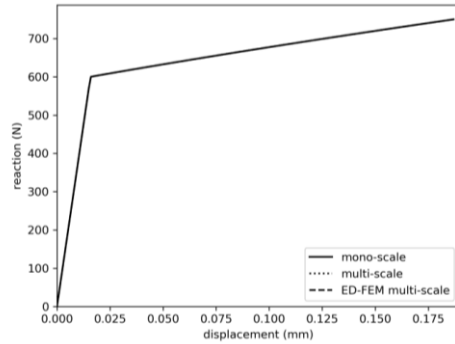


Fig. 11 Superposed force-displacement diagrams for elasto-damage with hardening computed by three different methods

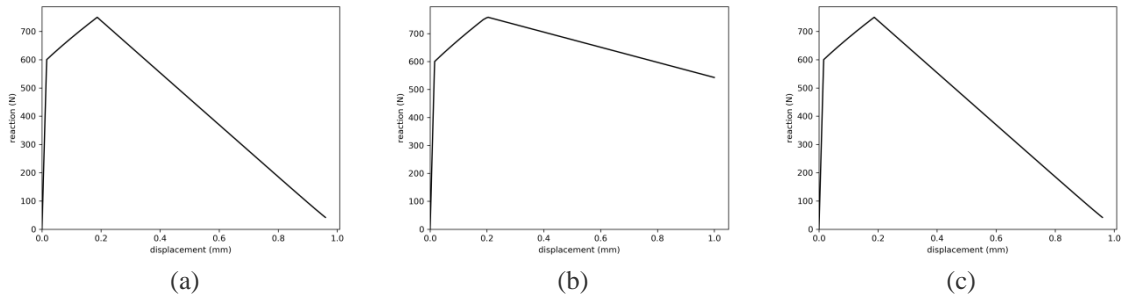


Fig. 12 Force-displacement diagrams for elasto-damage with softening: (a) Mono-scale; (b) Multi-scale; (c) ED-FEM multi-scale

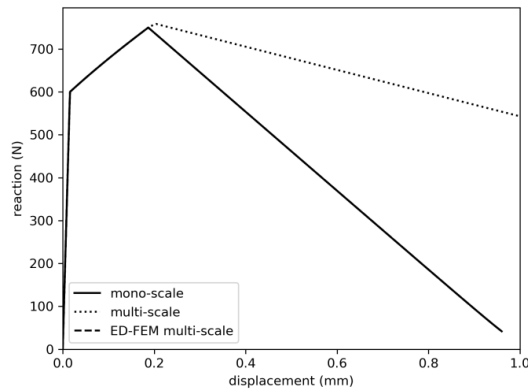


Fig. 13 Superposed force-displacement diagrams for elasto-damage with softening computed by three different methods

### 5.4 Elasto-damage with softening

When the value of the ultimate stress in the CST element is reached, a macro-crack appears and starts to open. The regular multi-scale method cannot transfer the displacement jump on the

macro-scale and therefore cannot produce the correct results. The micro-scale nodal displacement field on the interface is not computed correctly, which leads to a concentration of the stresses around the crack, and finally a collapse of the whole structure. That results in a force-displacement diagram shown in Fig. 12(b).

The proposed ED-FEM multi-scale method can transfer the displacement jump on the macro-scale and therefore allow the crack opening to increase until the stresses reach zero (as shown in 12(c)). The results for the mono-scale and ED-FEM multi-scale are the same for each time step of the analysis, and the values differ only after the fifth significant figure.

### 5.5 Validation examples of mesh objectivity

To prove that the proposed ED-FEM multi-scale method is not mesh dependent, we have tested it for two more examples with a different number of micro-scale mesh elements. In Fig. 14(a), the micro-scale mesh consists of  $6 \times 6$  CST elements, in Fig. 14(b) of  $18 \times 18$  elements and in Fig. 14(c) of  $54 \times 54$  CST elements. The weakened elements that are present only in the central macro-scale elements are again shown in gray.

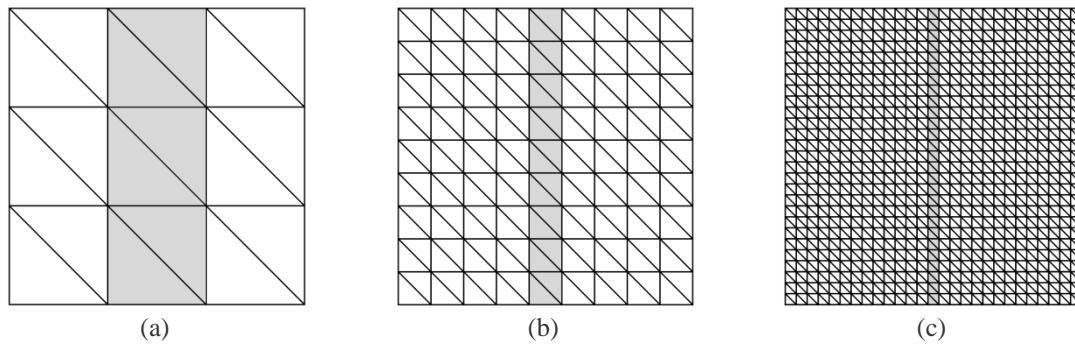


Fig. 14 Micro-scale mesh (a)  $6 \times 6$  elements; (b)  $18 \times 18$  elements; (c)  $54 \times 54$  elements

After running the ED-FEM multi-scale method examples with different micro-scale meshes, we have obtained the identical results for all three cases as shown in Fig. 15.

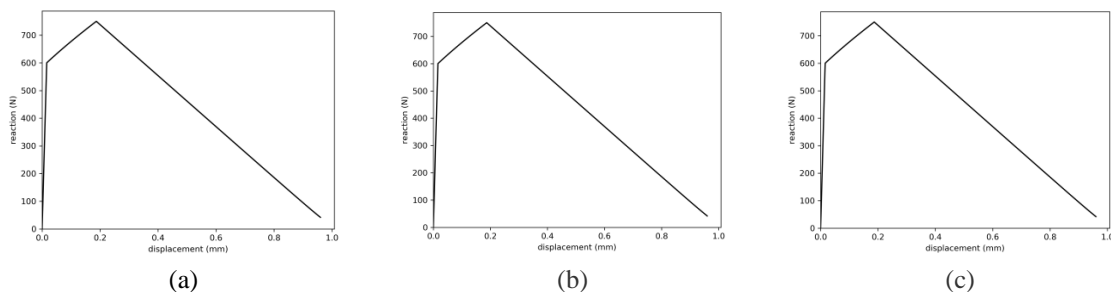


Fig. 15 Force-displacement diagrams for elasto-damage with softening for different number of micro-scale elements: (a)  $6 \times 6$  elements; (b)  $18 \times 18$  elements; (c)  $54 \times 54$  elements

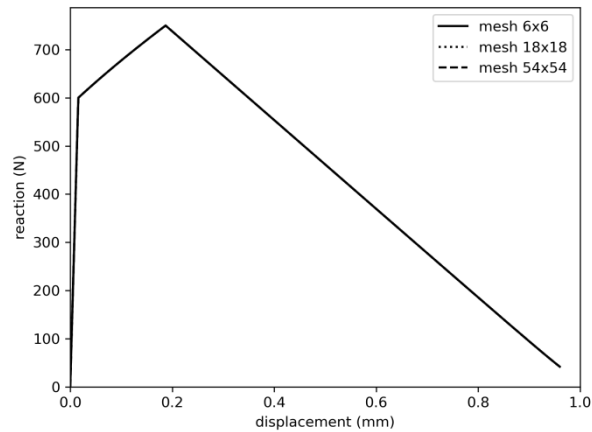


Fig. 16 Superposed force-displacement diagrams for elasto-damage with softening computed with different number of micro-scale elements

## 6. Conclusions

In this work, we have presented an improved version of a strong multi-scale coupling that can take into account localized failure. The crack opening on the macro-scale is modeled using the embedded strong discontinuity. It allows the computation to enter into the softening phase, where the damage occurs and the crack starts to propagate. The operator split procedure is introduced on the macro-scale to compute the nodal displacement field and the displacement discontinuity field. We have shown on a simple 2D tension test that the proposed method produces the same results as a benchmark mono-scale method, and shows an improvement for the softening phase compared to the previously developed multi-scale method.

The next step for improving this method would be to add the functionality of crack opening for both mode I and mode II (Do *et al.* 2017). In this way, a crack could occur and propagate at a certain angle, and some more complex examples, like the three-point bending test, could be executed. Additionally, the multi-scale coupling formulation can be adapted to work for localized failure in 3D.

## Acknowledgments

This work was supported jointly by Haut-de-France Region (CR Picardie) (120-2015-RDISTRUCT-000010 and RDISTRUCT-000010) and EU funding (FEDER) for Chaire-de-Mécanique (120-2015-RDISTRUCTF-000010 and RDISTRUCTI-000004). This support is gratefully acknowledged.

## References

Do, X.N., Ibrahimbegovic, A. and Brancherie, D. (2015), "Combined hardening and localized failure with softening plasticity in dynamics", *Coupled Syst. Mech.*, **4**(2), 669-690.

- Do, X.N., Ibrahimbegovic, A. and Brancherie, D. (2017), "Dynamics framework for 2D anisotropic continuum- discrete damage model for progressive localized failure of massive structures", *Comput. Struct.*, **183**, 14-26.
- Do, X.N. and Ibrahimbegovic, A. (2018), "2D continuum viscodamage-embedded discontinuity model with second order mid-point scheme", *Coupled Syst. Mech.*, **7**(6), 669-690.
- Feyel, F. and Chaboche, J.L. (2000), "FE2 multiscale approach for modelling the elastoviscoplastic behaviour of long fibre SiC/Ti composite materials", *Comput. Meth. Appl. Mech. Eng.*, **183**(3-4), 309-330.
- Geers, M.G.D., Kouznetsova, V.G. and Brekelmans, W.A.M. (2010), "Multi-scale computational homogenization: Trends and challenges", *J. Comput. Appl. Math.*, **234**(7), 2175-2182.
- Hautefeuille, M., Colliat, J.B., Ibrahimbegovic, A., Matthies, H.G. and Villon, P. (2012), "A multi-scale approach to model localized failure with softening", *Comput. Struct.*, **94**, 83-95.
- Ibrahimbegovic, A. and Markovic, D. (2003), "Strong coupling methods in multi-phase and multi-scale modeling of inelastic behavior of heterogeneous structures", *Comput. Meth. Appl. Mech. Eng.*, **192**(28-30), 3089-3107.
- Ibrahimbegovic, A. and Brancherie, D. (2003), "Combined hardening and softening constitutive model of plasticity: Precursor to shear slip line failure", *Comput. Mech.*, **31**(1-2), 88-100.
- Ibrahimbegovic, A. (2009), *Nonlinear Solid Mechanics, Theoretical Formulations and Finite Element Solution Methods*, Springer.
- Ibrahimbegovic, A., Kassiotis, C. and Niekamp, R. (2016), "Fluid-structure interaction problems solution by operator split methods and efficient software development by code-coupling", *Coupled Syst. Mech.*, **5**(2), 145-156.
- Niekamp, R., Markovic, D., Ibrahimbegovic, A., Matthies, H.G. and Taylor, R.L. (2009), "Multi-scale modelling of heterogeneous structures with inelastic constitutive behavior, part II-software coupling implementation aspects", *Int. J. Comput.-Aid. Eng. Softw.*, **26**(1-2), 6-28.
- Niekamp, R., Ibrahimbegovic, A. and Matthies, H.G. (2014), "Formulation, solution and CTL software for coupled thermomechanics systems", *Coupled Syst. Mech.*, **3**(1), 1-25.
- Park, K.C., Felippa, C.A. and Rebel, G. (2002), "A simple algorithm for localized construction of non-matching structural interfaces", *Int. J. Numer. Meth. Eng.*, **53**(9), 2117-2142.
- Sarfaraz, S.M., Rosic, B.V., Matthies, H.M. and Ibrahimbegovic, A. (2018), "Stochastic upscaling via linear Bayesian updating", *Coupled Syst. Mech.*, **7**(2), 211-232.
- Zienkiewicz, O.C., Taylor, R.L. and Zhu, J.Z. (2013), *The Finite Element Method: Its Basis and Fundamentals*, Elsevier.